UNIVERSITÉ DE GENÈVE

Archive ouverte UNIGE
https://archive-ouverte.unige.ch

Article scientifique | Article | 2024

Accepted version | Open Access

This is an author manuscript post-peer-reviewing (accepted version) of the original publication. The layout of the published version may differ .

Maximizing Nanoscale Downshifting Energy Transfer in a Metallosupramolecular Cr(III)–Er(III) Assembly

Poncet, Maxime Arnaud; Besnard, Céline; Jiménez, Juan-Ramón; Piguet, Claude

How to cite

PONCET, Maxime Arnaud et al. Maximizing Nanoscale Downshifting Energy Transfer in a Metallosupramolecular Cr(III)–Er(III) Assembly. In: Inorganic chemistry, 2024, vol. 63, n° 39, p. 18345–18354. doi: 10.1021/acs.inorgchem.4c02397

This publication URL: https://archive-ouverte.unige.ch/unige:180499
Publication DOI: 10.1021/acs.inorgchem.4c02397

© This document is protected by copyright. Please refer to copyright holder(s) for terms of use.

Publication: *Inorg. Chem.* **2024**, *63*, 18345-18354. DOI 10.1021/acs.inorgchem.4c02397

Maximizing Nanoscale Downshifting Energy Transfer in a Metallo-supramolecular Cr(III)-Er(III) Assembly

Maxime Poncet,[†] Céline Besnard,[‡] Juan-Ramón Jiménez*[§] and Claude Piguet*[†]

[†]Department of Inorganic and Analytical Chemistry, University of Geneva, 30 quai E. Ansermet, CH-1211 Geneva 4, Switzerland

[‡]Laboratory of Crystallography, University of Geneva, 24 quai E. Ansermet, CH-1211 Geneva 4, Switzerland.

[§]Departamento de Química inorgánica, Facultad de Ciencias, Universidad de Granada and Unidad de Excelencia en Química (UEQ), Avda. Fuente Nueva s/n, 18071, Granada, Spain.

KEYWORDS. Energy-transfer, chromium, supramolecular, lanthanide, luminescence

ABSTRACT: Pseudo-octahedral $Cr^{III}N_6$ chromophores hold a unique appeal for low-energy sensitization of NIR lanthanide luminescence due to their exceptionally long-lived spin-flip excited states. This allure persists despite the obstacles and complexities involved in integrating both elements into a metallosupramolecular assembly. In this work, we have designed a structurally optimized heteroleptic Cr^{III} building block capable of binding rare earths. Following a complex-as-ligand synthetic strategy, two heterometallic supramolecular assemblies, in which three peripherical Cr^{III} sensitizers coordinated through a molecular wire to a central Er^{III} or Y^{III}, have been prepared. Upon excitation of the Cr^{III} spin-flip states, the downshifted Er($^4I_{13/2}\rightarrow{}^4I_{15/2}$) emission at 1550 nm was induced through intramolecular energy transfer. Time-resolved experiments at room temperature reveal a $Cr^{III}\rightarrow Er^{III}$ energy-transfer of 62-73% efficiencies with rate constants of about $8.5x10^5$ s^{-1} despite the long donor-acceptor distance (*circa* 14 Å). This efficient directional intermetallic energy transfer can be rationalized using the Dexter formalism which is promoted by rigid linear electron-rich alkyne bridge that acts as a molecular wire connecting the Cr^{III} and Er^{III} ions.

INTRODUCTION

Luminescent lanthanide ions have a wide range of interest within the scientific community for their applications in biomolecule detection, as nanoprobes, in medical diagnosis, in telecommunication, lighting and energy conversion.[1-6] Some of the trivalent lanthanides exhibit NIR emission, which can be slightly modulated by their chemical environments, and significant endeavors have been devoted to the creation of materials possessing these highly effective optical properties.[7] In the NIR region, trivalent Neodymium (Nd^{III}, 9400 cm^{-1}), Thulium (Tm^{III}, 5000-5500 cm^{-1}), Ytterbium (Yb^{III}, 10000 cm^{-1}) and Erbium (Er^{III}, 6250-6600 cm^{-1}) are the most promising in terms of light emission.[8] Due to the parity-forbidden character of the f-f transitions, direct excitation of the lanthanides ions is very inefficient. The use of closed-shell organic ligands has been thus widely used for sensitization of NIR Ln^{III} luminescence through the so-called antenna effect.[9] This energy transfer (EnT), operating through Dexter-type double electron exchange, is achievable through the coordination of a ligand to the metal along with a short distance separating them. Nevertheless, when long wavelength light (VIS or NIR) is used to sensitize near-IR/IR luminescent lanthanides (*i.e.* Nd^{III}, Yb^{III} or Er^{III}), d-block chromophores acting as energy harvesters are particularly appealing due to their (i) usually long-lived excited state, which ensures more time for inducing the energy transfer to the f-block metal ion, (ii) customizable emission and absorption energies (iii) limited sensitivity to photobleaching and (iv) efficient intermetallic communication via directional energy transfer. With this in mind, several polymetallic edifices exploiting precious and inert 4d (Ru^{II} and Pd^{II}) and 5d (Os^{II}, Ir^{III} and Pt^{II}) and their long-lived ^{3}MLCT have been proved to sensitize quite efficiently NIR Ln^{III} luminescence.[10-18] However, the low abundance and high cost of those transition metals represent an important drawback for the development of cost-effective energy converting materials. Within the 3d series, the earth abundant Cr^{III}, embedded within a pseudo-octahedral ligand field, has demonstrated to be an attractive sensitizer which benefits from (i) favorable inertness, (ii) low cost and long-lived excited states.[19-22] However, synthetic pathways able to combine several chromium-polypyridyl units and Ln^{III} within an energy converter single (supra)molecule are scarce and dominated by serendipitous synthetic methods.[23-35] Mostly, d-f arrays incorporating cyanido-bridged Cr^{III}-CN-Ln^{III} moieties such as {[Cr(CN)$_4$(μ-CN)$_2$Ln(H$_2$O)$_2$(dmf)$_4$]}$_\infty$ (dmf = dimethylformamide) where the Ln = Yb^{III} or Nd^{III} have been described by Ward and co-workers.[33] In these systems, the Cr^{III} act as sensitizer for the NIR lanthanide luminescence via a Dexter EnT mechanism with an impressive rate constant $k_{Cr\rightarrow Ln} = 10^8$ s^{-1} (Figure 1a). Kaizaki and co-workers also described very efficient short distance EnT via oxalate bridging units in [(acac)$_2$Cr(ox)Ln(HBpz$_3$)$_2$] (Ln = Nd^{III}, Yb^{III} or Er^{III}; acac = acetylacetonate; HBpz$_3$ = tris(pyrazol-1-yl)borate, Figure 1b).[24] In both cases and at low temperature, only partial EnT occurs whereas at room temperature a close-to-quantitative thermally activated EnT was observed providing only Ln centred emission. Long distance intermetallic downshifting phenomena between Cr^{III} (sensitizer) and Ln^{III} (activators: Yb^{III} or Nd^{III}) has also been established in triple-stranded helicates with simplified chemical formula [CrLn(**py-bzimpy**)$_3$]$^{6+}$ and [CrLnCr(**dipy-pybzimpy**)$_3$]$^{9+}$.[25] In these systems, long-range electron dipole-dipole formalism (Förster mechanism) was applied for analysing the rate constants of the energy transfer and the measured $k_{Cr\rightarrow Ln}$ amounts to 232-456 s^{-1},[29-32] The longer distance between the sensitizer and the activator and their poor orbital overlap are responsible for the much lower intramolecular EnT rate constants ($k_{Cr\rightarrow Ln} = 10^2$-$10^3$ s^{-1}) compared to the electronic communication mediated by short molecular bridges such as oxalate and cyanide ($k_{Cr\rightarrow Ln} = 10^7$-$10^8$ s^{-1}). Under slow energy transfer regime, the total observed decay rate constant of the excited level of the donor (sensitizer) $\boldsymbol{k_{obs}^{Donor} = k_{relax}^{D} + k_{D\rightarrow A}^{EnT}}$ may be largely dominated by the decay rate constant of the acceptor (luminophore, $\boldsymbol{k_{obs}^{Acceptor} \gg k_{obs}^{Donor}}$) and the emission lifetime of the acceptor mirror that of the donor. This situation occurs for the above-mentioned triple helicates, where the electronic communication between the chromium donor and the lanthanide acceptor is limited and the final NIR Nd^{III} and Yb^{III}-based emission,

usually displaying microsecond lifetimes, reaches the millisecond regime characteristic of the long-lived Cr^{III} donors (Figure 1c).[29] Moreover, in these helicates, selective intense irradiation of Cr^{III} produces an Energy Transfer Upconversion (ETU) with the detection of the Er($^4S_{3/2}\rightarrow{}^4I_{15/2}$) green luminescence at 543 nm (18400 cm^{-1}) following near infrared excitation. Finally, and despite the long distance between the Yb^{3+} and Cr^{3+} (*circa* 9 Å) and the non-bonding between the two complexes in the crystalline chromium-ytterbium ionic salt of general formula [Yb(**dpa**)$_3$][Cr(ddpd)$_2$] (dpa = dipicolinate, ddpd = N,N'- dimethyl-N,N'-dipyridin-2-ylpyridine-2,6-diamine), a non-negligible Cr→Yb EnT could be detected in the solid state.[36] Interestingly, Cr^{III} upconversion was also observed upon pumping Yb^{III} centers through a Cooperative Upconversion (CU) mechanism.[36]

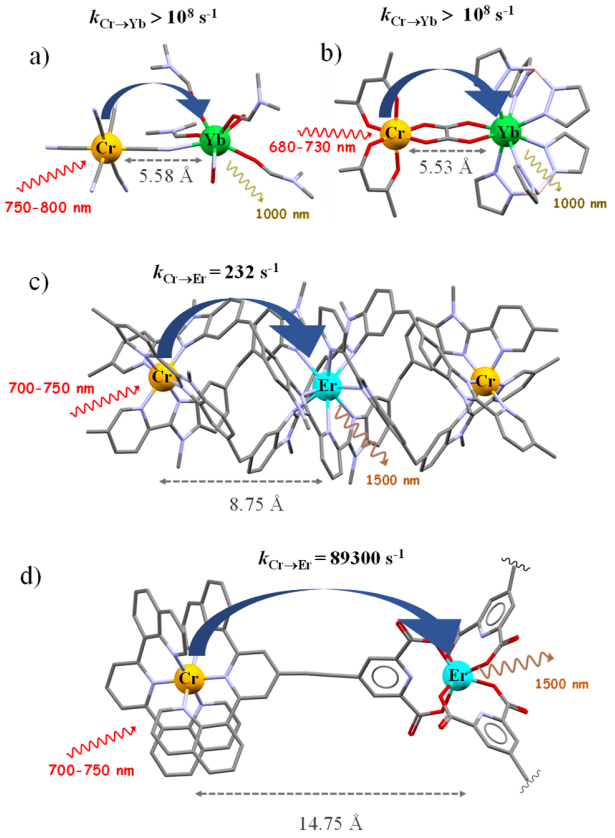

Figure 1. Molecular structures of some assemblies containing Cr-Ln moieties with their respective energy transfer rate constants controlling NIR lanthanide downshifted emission; Hydrogen atoms and counter ions omitted for clarity. Color codes: Cr (orange), N (blue), C (gray), O (red), Yb (gren) and Er (blue). a) {[Cr(CN)$_4$(μ-CN)$_2$Yb(H$_2$O)$_2$(dmf)$_4$]}$_\infty$,[33] b) [(**acac**)$_2$Cr(**ox**)Yb(**HBpz**$_3$)$_2$],[24] c) [CrErCr(**dipy-pybzimpy**)$_3$]$^{9+}$ [29] and d) [(**dqp**Cr**L1**)$_3$Er]$^{6+}$ reported in this work.

Apart from these remarkable examples, a complex-as-ligand strategy has been tentatively applied by our group to construct 3d based polymetallic assemblies,[37,38] but the construction of 3d-4f assemblies remains underexplored. In this work, we report on the synthesis and characterization of a novel heteroleptic Cr^{III} building block, [Cr(**dqp**)(H$_2$-**L1**)]$^{3+}$, where **dqp** is 2,6-di(quinolin-8-yl)pyridine and H$_2$-**L1** contains a dqp unit linked through an alkyne bridge to a dipicolinic acid. Reaction between the building block and a lanthanide ion Er^{3+} or Y^{3+} led to the formation of a hetero-tetrametallic assembly (Figure 1d). The full structural, solution and photophysical analysis of the assembly is analysed and reported here.

RESULTS AND DISCUSSION

Synthesis and characterization of the ditopic ligand 10. The synthesis of the ditopic ligand, **10**, was achieved following the multistep scheme depicted in Figure 2 (Appendix 1 in ESI for synthetic details). Starting with 2,6-dibromopyridine (**1**), an iridium-catalyzed activation followed by borylation and subsequent oxidation of the carbon-boron bond with the triple salt *oxone*® (**2** $KHSO_5{\cdot}KHSO_4{\cdot}K_2SO_4$) afforded 2,6-dibromopyridin-4-ol (**2**).[39] Straightforward protection of the alcohol with methyl iodide yielded 2,6-dibromo-4-methoxypyridine (**3**) that was further combined with quinoline-8-boronic acid in a Suzuki coupling under microwave conditions to yield **4**.[40] Once **4** was isolated, the methoxy group was replaced by a –Br group,[41,42] giving **dqp**-Br (**5**). Separately, 8,8'-(4-ethynylpyridine-2,6-diyl)diquinoline (**6**) was synthesized from **5** by Sonogashira cross-coupling.[43,44] The dipicolinate-moiety was synthesized starting from chelidamic acid (**7**) that was reacted with PBr_5 to yield diethyl 4-bromopyridine-2,6-dicarboxylate (**8**).[45] After Sonogashira cross-coupling, diethyl 4-ethynylpyridine-2,6-dicarboxylate (**9**) was achieved and could then be coupled with **5** using a second Sonogashira coupling reaction to yield **10** as supported by ^{1}H NMR spectroscopy (Figure S1).

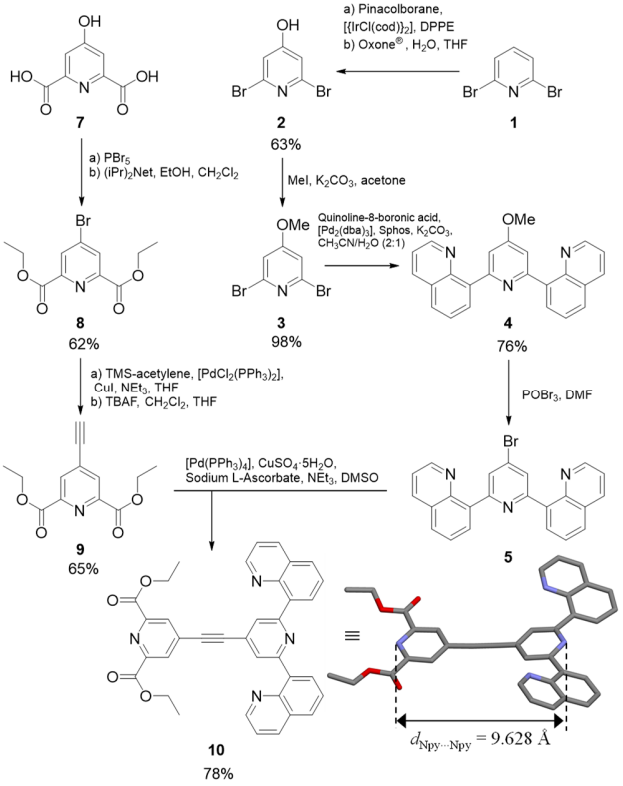

Figure 2. Multistep synthetic scheme for preparing the ditopic ligand diethyl 4-((2,6-di(quinolin-8-yl)pyridin-4-yl)ethynyl)pyridine-2,6-dicarboxylate (**10**). Its molecular structure, as found in the crystal structure, is highlighted; color codes: N (blue), C (gray), O (red),

Slow evaporation of a concentrated ethylacetate solution containing the ligand yielded single crystals of **10** suitable for X-Ray Diffraction (XRD) (Figures 2 and S2-S3, Tables S1-S3). The nitrogen atoms of each of the two quinolines from the **dqp** moiety are facing the opposite direction as the central nitrogen atom on the pyridine (*transoid* arrangement of the terimine N^N^N ligand, Figures 2 and S2). The two quinolines arms are slightly out of the plane of the central pyridine (19.6° and 31.6°) because of the steric crowding implying the hydrogen atoms on the central pyridine and those of the connected appended quinoline rings that prevents perfect

planarity (Figure S3). As a consequence of the triple bond located in the middle of the molecule extending π-delocalization, the two connected pyridine rings are almost coplanar (dihedral angle = 7.65°). The distance between the two coordinating nitrogen atoms on each central pyridine amounts to 9.628(3) Å, which allows a first rough estimation of Cr-Ln distances expected in the target final assemblies ($d_{Cr\text{-}Ln}$ ~ 0.2(Cr-N bond) + 0.96 ($N_{py}\cdots N_{py}$) + 0.25 (N-Ln bond) ≈ 1.4 nm).

Synthesis, structure and spectroscopic properties of heteroleptic complex-as-ligand [Cr(dqp)(H₂-L1)](CF₃SO₃)₃. The heteroleptic [Cr(**dqp**)(H₂-**L1**)]$^{3+}$ complex (**L1**$^{2-}$ = 4-((2,6-di(quinolin-8-yl)pyridin-4-yl)ethynyl)pyridine-2,6-dicarboxylate) was prepared by following a previous synthetic strategy described by our group (Figure 3a and Appendix 1 in the ESI for synthetic details).[46,47] Firstly, the neutral halogeno-complex, [Cr(**10**)Cl₃] could be obtained by reacting commercially available Cr(THF)₃Cl₃ with the tridentate ligand **10** in isopropanol under microwave conditions at 140°C. The green compound was isolated, washed and characterized. Addition of 3 equivalents of $AgSO_3CF_3$ in acetonitrile led to the soluble intermediate [Cr(**10**)$(SO_3CF_3)_3$]. While exploiting the known lability of the Cr-OSO_2CF_3 bond,[48] 1 eq. of **dqp** ligand was added to the mixture and after heating under microwave irradiation, the heteroleptic [Cr(**dqp**)(**10**)]$(SO_3CF_3)_3$ complex was obtained (see Appendix 1 in the ESI for details). Upon solubilization of [Cr(**dqp**)(**10**)]$^{3+}$ in water, both ethyl esters could be carefully hydrolysed "on-the-complex" with an excess of sodium hydroxide that was neutralized after the reaction with HSO_3CF_3 leading to [Cr(**dqp**)(H₂-**L1**)]$^{3+}$. The mass spectrum of the complex displays specific peaks corresponding to [Cr(**dqp**)(H₂-**L1**)]$(SO_3CF_3)_2]^+$ and [Cr(**dqp**)(H₂-**L1**)]$(SO_3CF_3)]^{2+}$ centered at *m/z* = 1205.105 Da and 528.075 Da, respectively (Figure S4 and Table S4). Upon slow evaporation of a concentrated solution of [Cr(**dqp**)(H₂-**L1**)]$^{3+}$ in water, monocrystals of [Cr(**dqp**)(H₂-**L1**)]$(SO_3CF_3)_3\cdot 3.5H_2O$ suitable for X-ray diffraction were obtained (Figures 3 and S5-S7, Tables S5-S6). The Cr−N bond lengths are similar to those found in related polypyridyl Cr^{III} complexes, and the N(terminal)-Cr-N(terminal) bite angles of 176.36(8)° (Tables S5 and S6) are in agreement with the values obtained for the parent homoleptic [Cr(**dqp**)₂]$^{3+}$ complex and its analogues.[49,50] Similar to the latter complexes, π-stacking between the **dqp** and H₂-**L1** bound ligands can be appreciated by the relatively short distance between the two respective quinoline centroids ($d^1_{\mathbf{dqp-L1}}$=3.351 Å and $d^2_{\mathbf{dqp-L1}}$=3.386 Å) (Figure S6). The minor interplanar angles between the quinoline rings of **dqp** and **L1** ligands (17.78° and 19.28°) comfort the concept of intramolecular interligand π-stacking as a non-negligible driving force for the complexation process (Figure S7). The Cr···N_{py}(dipicolinate) distance amounts to 11.465(3) Å, which allows to refine and confirm the estimation of Cr-Ln distances expected in the target final assemblies to $d_{Cr\text{-}Ln}$ =1.1465 + 0.25 (N-Ln bond) = 1.4 nm. Interestingly, the terminal tridentate O^N^O dipicolinic acid binding unit grants the possibility to deprotonate the oxygen atoms, resulting in a doubly negatively charge site, entirely in favour of the complexation of a triply positively charged Ln^{III} ion.

The absorption spectrum of [Cr(**dqp**)(H₂-**L1**)]$^{3+}$ in acetonitrile shows maxima between 280 and 350 nm ($\varepsilon > 10^3$ $M^{-1}\cdot cm^{-1}$), which can be attributed to standard intense π*←π transitions, together with bands of lower intensities between 350 and 500 nm (ε < 103 $M^{-1}\cdot cm^{-1}$) assigned to mixed metal-centered and ligand-to-metal charge transfer (MC)/LMCT transitions (Figure 3b). The weak transitions located at even lower energies (500−600 nm) are ascribed to the spin-forbidden ^{3}π*←π transitions (Figure 3b). According to Time Dependent Density Functional Theory (TD-DFT) calculations on the parent [Cr(**dqp**)₂]$^{3+}$ compound,[48] the shoulder at 401 nm can be ascribed to the ligand field transition Cr($^4T_2$←$^4A_2$) leading to an estimated ligand field splitting of 25000 cm^{-1}. Upon excitation at 350 nm, within the ligand centered transitions, [Cr(**dqp**)(H₂-**L1**)]$^{3+}$ displays a narrow dual emission with maxima at 730 nm (13698 cm^{-1}) and 755 nm (13245 cm^{-1}) assigned to the spin-flip Cr(^2E,$^2T_1$→$^4A_2$) transitions (Figure 3b). The emission bands maxima are slightly red-shifted by 150 cm^{-1} compared to the parent [Cr(**dqp**)₂]$^{3+}$ complex. This drift can be reasonably assigned to a larger nephelauxetic effect produced by improved electronic delocalization onto the extended H₂-**L1** ligand in the heteroleptic analogue [Cr(**dqp**)(H₂-**L1**)]$^{3+}$.[51] The measured quantum yields for the latter complex amount to 16% and 0.3% in acetonitrile at room temperature under anaerobic and aerobic conditions, respectively, which are among the highest values reported for Cr(III) complexes.[52,53] The two spin-flip transitions share the same lifetime of about 1.62(6) ms in deaerated acetonitrile solution demonstrating a thermally equilibrated states at room temperature (Figure S13). At 77K, the high-energy emission band vanishes and only the lowest low-lying microstate is populated and detectable together with its vibrational progression. The low temperature excited state lifetime amounts to 2.63(7) ms in frozen H₂O/DMSO (1:1) solution (Figure S14). The excitation spectra recorded upon monitoring the emission bands at 748 and 728 nm match the absorption spectrum, demonstrating the participation of π-π*, LMCT, and LMCT/MC excited states for feeding the emissive Cr-centered doublet states (Figure 3b).

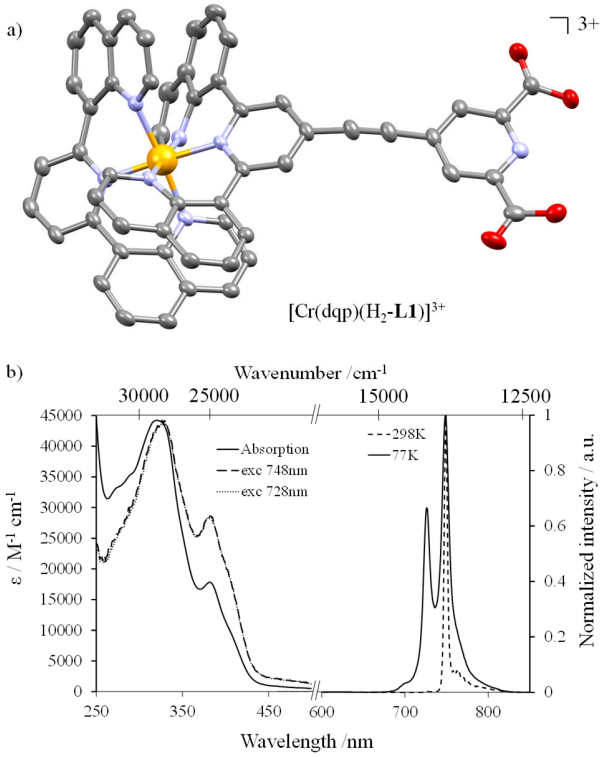

Figure 3. a) Molecular structure of the cationic complex as found in the crystal structure of [Cr(**dqp**)(H₂-**L1**)]$(SO_3CF_3)_3\cdot 3.5H_2O$. Ellipsoids plotted at the 50% probability level, hydrogen atoms and counter ions are omitted for clarity (CCDC 2361449.). Color codes: Cr (orange), N (blue), C (gray), O (red). b) Emission, absorption and excitation spectra of [Cr(**dqp**)(H₂-**L1**)]$^{3+}$ in acetonitrile solution at room temperature.

Synthesis and solution studies of the [(dqpCrL1)₃Ln]$^{6+}$ (Ln = Er^{3+} and Y^{3+}) assemblies. The supramolecular [(**dqp**Cr**L1**)₃Ln]$(SO_3CF_3)_6$ assemblies (Ln = Er^{3+} or Y^{3+}) are obtained by reacting the doubly deprotonated heteroleptic complex-as-ligand [**dqp**Cr**L1**]$^+$, obtained via the reaction of 1 eq. of

$[Cr(\mathbf{dqp})(H_2\text{-}\mathbf{L1})]^{3+}$ in presence of 2 eq. of *N*,*N*-diisopropylethylamine, with stoichiometric amount (3:1) of the lanthanide triflate salt in acetonitrile at room temperature (Figure 4a and Appendix 1 in the ESI for synthetic details). Slow precipitation induced by the diffusion of diethyl ether provides an orange precipitate that was filtered, washed with diethyl ether and dried. Despite countless crystallization attempts, single crystals suitable for X-ray diffraction could not be obtained. However, the spectrophotometric titration combined with speciation experiments and ESI-MS spectra support the formation and stability of the multimetallic $[(\mathbf{dqp}CrL1)_3Er]^{6+}$ and $[(\mathbf{dqp}CrL1)_3Y]^{6+}$ assemblies in solution. The mass spectra of the $[(\mathbf{dqp}CrL1)_3Ln]^{6+}$ (Ln = Er or Y) display similar pattern and gave excellent agreement with the theoretical isotopic distributions for the molecular ion (Figure 4, Figures S8-S11 and Tables S7- S8). It is worth stressing here that the final assemblies are prone to dimerization in the gas phase, probably as a result of the presence of triflate counter-anions which are able to link two cationic units via their accessible and shared central lanthanide cations (Figure 4 bottom).

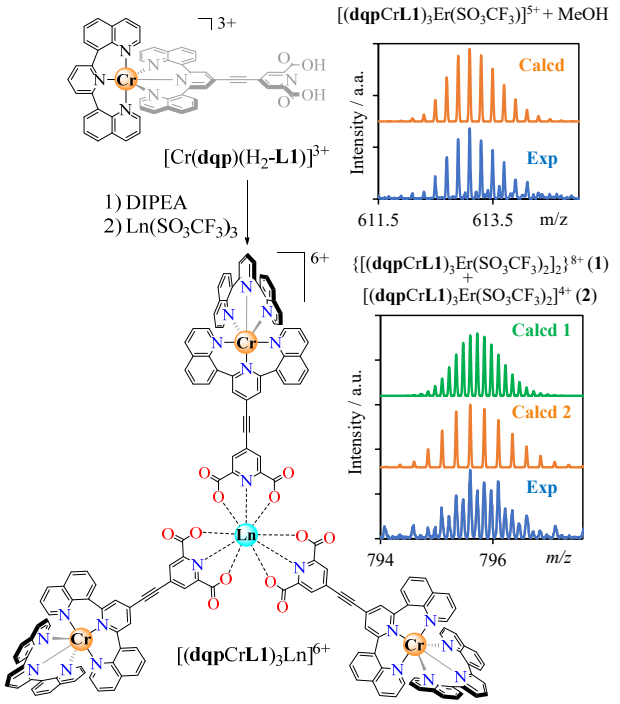

Figure 4. Synthesis of $[(\mathbf{dqp}CrL1)_3Ln]^{6+}$ assemblies from $[Cr(\mathbf{dqp})(H_2\text{-}\mathbf{L1})]^{3+}$ and associated HR-ES/MS spectra.

The complexation and stability constants of the complex-as-ligand $[\mathbf{dqp}CrL1]^+$ with a trivalent lanthanide ion was analysed by spectrophotometric titrations because of the incompatibility of the slow electronic relaxation of Cr(III) complexes with high-resolution NMR techniques. $[\mathbf{dqp}CrL1]^+$ was stepwise titrated with $Ln(SO_3CF_3)_3$ (Ln = Er^{3+} or Y^{3+}) in dry acetonitrile. After each addition, a timeout of one minute was carried to ensure that thermodynamic equilibrium is reached. At each point, an absorption spectrum of the solution was recorded. After data treatment based on evolving factor analysis as implemented in the software ReactLab™ Equilibria,[54-57] two sets of three stability constants, corresponding to the formation of 1:1, 1:2 and 1:3 complexes, could be extracted (eqs 1-3).

$$Ln^{3+} + [\mathbf{dqp}CrL1]^+ \overset{\beta_1}{\rightarrow} [(\mathbf{dqp}CrL1)Ln]^{4+} \quad (1)$$

with $\log(\beta_1)$ = 9.177 ±0.016 for Ln = Er^{3+} and $\log(\beta_1)$ = 7.467 ±0.005 for Ln = Y^{3+}

$$Ln^{3+} + 2 \cdot [\mathbf{dqp}CrL1]^+ \overset{\beta_2}{\rightarrow} [(\mathbf{dqp}CrL1)_2Ln]^{5+} \quad (2)$$

with $\log(\beta_2)$ = 16.912 ±0.031for Ln = Er^{3+} and $\log(\beta_2)$ = 13.888 ±0.009 for Ln = Y^{3+}

$$Ln^{3+} + 3 \cdot [\mathbf{dqp}CrL1]^+ \overset{\beta_3}{\rightarrow} [(\mathbf{dqp}CrL1)_3Ln]^{6+} \quad (3)$$

with $\log(\beta_3)$ = 23.403 ±0.045 for Ln = Er^{3+} and $\log(\beta_3)$ = 19.386 ±0.012 for Ln = Y^{3+}

The significant increases of the formation constants with decreasing effective ionic radii in going from Y^{3+} to Er^{3+} is in line with the standard electrostatic trend reported for $[Ln(dipicolinate)_n]^{(3-2n)+}$ (*n* = 1-3) along the lanthanide series.[58,59] A simulation of the speciation in solution using HySS software [60] for a target 1 mM solution of $[(\mathbf{dqp}CrL1)_3Ln]^{6+}$, *i.e* the concentration at which the photophysical experiments were run, shows that 96.5% of the complex-as-ligand is involved in the $[(\mathbf{dqp}CrL1)_3Er]^{6+}$ and 89.5% in $[(\mathbf{dqp}CrL1)_3Y]^{6+}$ (Figure 5).

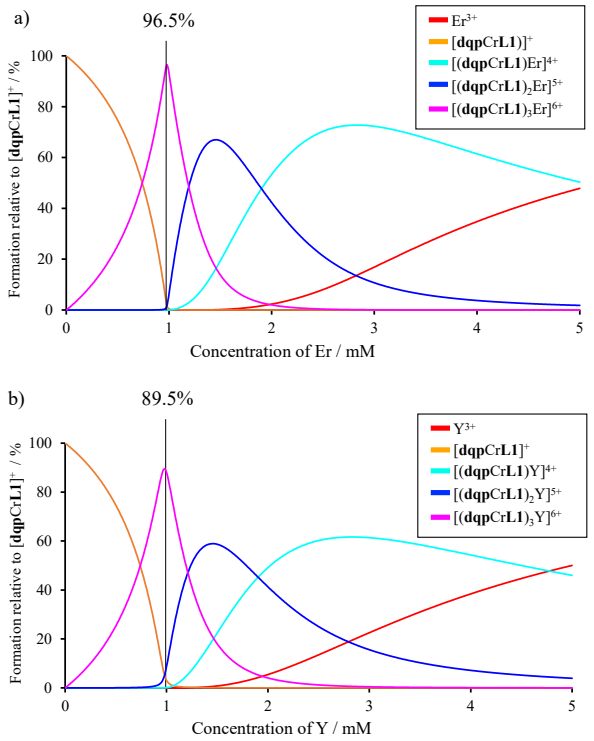

Figure 5. Simulated speciations relative to $[\mathbf{dqp}CrL1]^+$ and using the formation constants pertinent to eqs (1-3). a) Titration of a 3 mM solution of $[\mathbf{dqp}CrL1]^+$ with $Er(SO_3CF_3)_3$ in CH_3CN. ($c_{[(\mathbf{dqp}CrL1)_3Er]}$ = 1 mM) and b) simulation of a titration of a 3 mM solution of $[\mathbf{dqp}CrL1]^+$ with $Y(SO_3CF_3)_3$ in CH_3CN ($c_{[(\mathbf{dqp}CrL1)_3Y]}$ = 1 mM).

Absorption, emission, and energy transfer properties of the $[(\mathbf{dqp}CrL1)_3Ln]^{6+}$ assemblies. The UV absorption spectra of the assemblies were recorded at millimolar concentration using a 0.2 mm pathlength cuvette (Figure 6). As expected, the total ε values of the d-f complexes are 3 times larger than those of the deprotonated $[\mathbf{dqp}Cr(\mathbf{L1})]^+$ since they involve three such units in their molecular formula (Figure 6a). The UV region is dominated by the presence of $\pi^* \leftarrow \pi$ ligand-centred transitions of the organic backbone whereas the transitions at lower energies in the 300-400 nm range (27000 cm^{-1} and 20000 cm^{-1} respectively) are attributed to a mixed of Ligand-to-Metal Charge Transfers (LMCT), Metal-Centered (MC) and a fraction of Metal-to-Ligand Charge Transfers (MLCT), similarly to the isolated $[Cr(\mathbf{dqp})(H_2\text{-}\mathbf{L1})]^{3+}$ precursor (Figure 3b). Upon recording the absorption spectra in the near

infrared region (NIR, up to 1600 nm) in concentrated acetonitrile solutions, the parity-forbidden f-f and parity- and spin-forbidden d-d transitions were detected (Figure 6b). The radiative rate constant (k_{rad}) for the d-d and f-f transitions in the assemblies were calculated by the integration of the band absorptions and following the Strickler-Berg equation (4).[61,62]

$$k_{rad}^{Cr\ or\ Er} = \frac{1}{\tau_{rad}^{Cr\ or\ Er}} = 2303 \times \frac{8\pi c n^2 \tilde{\nu}^2 g_{GS}}{N_A g_{ES}} \int \varepsilon(\tilde{\nu}) d\tilde{\nu} \qquad (4)$$

in which, n is the refractive index (n_{CH3CN} = 1.33), $\tilde{\nu}$ the barycentre of the transition, N_A Avogadro's number. The two terms g_{ES} and g_{GS} are the degeneracy of the excited state and the ground state levels respectively. In the case of the trivalent chromium atom, g_{GS} = 4, g_{ES} = 4 for the ^2E level and g_{ES} = 6 for the $^2T_1$ level. For the trivalent erbium atom, $g_{GS} = (2J+1)$ and $g_{ES} = (2J'+1)$. Finally, the $\int \varepsilon(\tilde{\nu}) d\tilde{\nu}$ is the integral of the absorption band (in cm^2). The computed values are gathered in Table 1. In both [(**dqp**Cr**L1**)$_3$Er]$^{6+}$ and [(**dqp**Cr**L1**)$_3$Y]$^{6+}$, the k_{rad}^{Cr} for the spin-flip transitions are in line with the parent [Cr(**dqp**)$_2$]$^{3+}$ compound.[49]

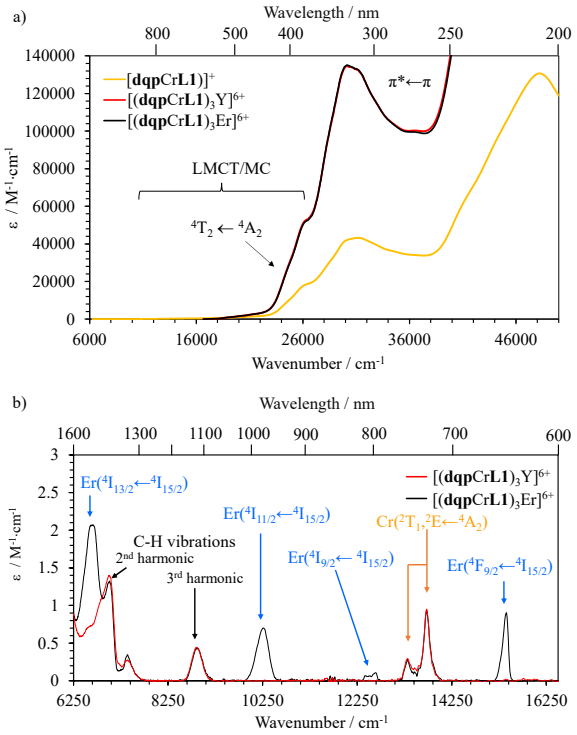

Figure 6. a) UV absorption spectra recorded in acetonitrile at 1 mM for [(**dqp**Cr**L1**)$_3$Er]$^{6+}$ (black trace), [(**dqp**Cr**L1**)$_3$Y]$^{6+}$ (red trace) and [**dqp**Cr(**L1**)]$^+$ (yellow trace) in a 0.2 mm cuvette. b) Absorption spectra of the tetra-metallic species in the (near) infrared region of the electromagnetic spectrum at 1 mM in acetonitrile.

Upon excitation of the tetra-metallic assemblies at 350 nm, the typical emission bands Cr($^2T_1 \rightarrow {}^4A_2$), Cr($^2E \rightarrow {}^4A_2$) in both [(**dqp**Cr**L1**)$_3$Y]$^{6+}$ and [(**dqp**Cr**L1**)$_3$Er]$^{6+}$, as well as Er($^4I_{13/2} \rightarrow {}^4I_{15/2}$) in the latter complex, have been recorded in the solid state and solution at variable temperatures (10K-298K). In both systems, the room temperature Cr-based dual emission observed at 730 nm (13730 cm^{-1}) and 755 nm (13350 cm^{-1}) slowly evolves towards a single emission from the Cr(^2E) level at low temperature (Figure 7a). It can be reasonably assumed that the $^2T_1$ level starts to be populated from 90 K upwards, preventing any thermal population through internal conversion between the $^2T_1$ and the ^2E level at lower temperature. For [(**dqp**Cr**L1**)$_3$Er]$^{6+}$, the broad and structured emission located at 1500-1600 nm correspond to the characteristic Er($^4I_{13/2} \rightarrow {}^4I_{15/2}$) transition. Upon decreasing the temperature, the low-lying microstate is populated as a consequence of a thermal equilibration at 10 K (Figure 7a). As it is confirmed each emissive transition's excitation spectra match the absorption spectra of the corresponding compound (Figure S12).

To investigate the electronic communication between the Cr^{III} and Er^{III} ions, steady-state and time resolved experiments were carried out. For this purpose, a continuous-wave laser at 730 nm was used to hit the Cr($^2T_1 \leftarrow {}^4A_2$) spin-flip band, thus bringing the 3d metal centre into its Cr($^2T_1$) excited state. If the EnT takes place, the *quasi*-isoenergetic Er($^4I_{9/2}$) level will be populated to quickly relax to the long-lived Er($^4I_{13/2}$) energy level, from which the typical NIR emission of the erbium might be observed (Figure 7b). The evolution of the emission from the Er($^4I_{13/2}$) level upon spin-flip excitation (at 730 nm) was observed at different temperatures indicating a successful Cr→Er light-downshiting (Figure 7 b,c). The efficiency of the intermetallic energy transfer is related to the excited state lifetimes of the donor Cr^{3+} in the presence of the acceptor in [(**dqp**Cr**L1**)$_3$Er]$^{6+}$, compared with that in absence of acceptor as measured in [(**dqp**Cr**L1**)$_3$Y]$^{6+}$ (eq 5).

$$\eta_{Cr \rightarrow Er} = 1 - \frac{\tau_{CrEr}}{\tau_{CrY}} \qquad (5)$$

In acetonitrile solution at room temperature, the radiative decay is mono-exponential and the associated excited state lifetime of the Cr^{III} center drops from 40.7 µs to 13.8 µs in going from [(**dqp**Cr**L1**)$_3$Y]$^{6+}$ to [(**dqp**Cr**L1**)$_3$Er]$^{6+}$ (Figures S17-S18) which result in an EnT efficiency ($\eta_{Cr \rightarrow Er}$) of 66%. Similar behaviour was found in the solid state, with values of 31.2 µs and 8.2 µs (Figure S15-S16), respectively, giving a 73% efficiency for the downshifting energy transfer. The rate of the energy transfer, $k_{Cr \rightarrow Er}$, could be calculated using eq (6)

$$k_{Cr \rightarrow Er} = \frac{1}{\tau_{CrEr}} - \frac{1}{\tau_{CrY}} \qquad (6)$$

from which exceptional values of 47900 and 89300 s^{-1} in solution and in solid state respectively were computed at room temperature. This demonstrates the efficient and fast phonon-assisted EnT between the donor and the acceptor which is mediated by the alkyne bridge despite the long distance (*circa* 1.4 nm). A Dexter-type mechanism promoted by the alkyne bridge and some non-negligible overlap of the wave function of the excited state of the donor and the acceptor are probably at the origin of such an efficient EnT.

It is noteworthy that, as temperature decreases, both the efficiency (Figure S19) and the rate of energy transfer (Figure 8) decrease in solution and in the solid state. This is in line with a temperature-dependent energy transfer phenomenon, commonly observed in dominant Dexter energy transfer processes.

Finally, the luminescence quantum yield for the emission of Er upon sensitization of the spin-flip band of Cr was calculated to be 0.063% with eq (7)

$$\phi = \eta_{Cr \rightarrow Er} \times \phi_{Er}^{Er} \qquad (7)$$

where the ϕ_{Er}^{Er} is the intrinsic quantum yield. The latter parameter reflects the extent of non-radiative deactivation processes occurring through interactions with the surroundings of the metal ion and it is estimated as the ratio between τ_{obs} and τ_{rad} of [(**dqp**Cr**L1**)$_3$Er]$^{6+}$ at 1530 nm (Table 1). Only few Cr^{III}-Er^{III} compounds have been reported in the literature, most of them using cyanide bridges to put the metals in communication.[26-28,32,35,64-67] The presented [(**dqp**Cr**L1**)$_3$Er]$^{6+}$ displays the longest intermetallic distance among them. The kinetic study of the intramolecular energy transfer between Cr^{III} and Er^{III} is even more scarce and carried out in the trimetallic [CrErCr(**dipy-pybzimpy**)$_3$]$^{9+}$ (Figure 1c), and in the

corresponding bimetallic assembly.[68-69] The rate constant obtained reach the 10^2 s^{-1} range for an intermetallic distance of *circa* 9.3 Å with makes the present system 200-400 times faster despite the longer intermetallic distance (*circa* 14 Å). More largely, only a handful of heterometallic Cr^{III}-Ln^{III} molecular assemblies were kinetically studied, and the rate of energy transfer calculated.[24,27,29,31-33,70-71] Because the energy rate transfer strongly depends on the overlap integral between the emission spectra of the donor and the absorption spectra of the acceptor, typical values found in the literature for Cr^{III}-Nd^{III} and Cr^{III}-Eu^{III} are in the 10^3 s^{-1} range for an intermetallic distance of *circa* 9.3 Å.[27, 29, 31-32, 70] In these systems, the energy transfer mainly operates through a Förster-type mechanism. To compare the $[(\mathbf{dqp}Cr\mathbf{L1})_3Er]^{6+}$ with another system operating through Dexter energy transfer, Lazarides *et al.* studied a cyano-bridged Cr^{III}-Yb^{III} system with an intermetallic distance of 5.59 Å.[33] The rate of energy transfer was estimated to be greater than 10^8 s^{-1}. The herein reported supramolecular assembly is, to the best of our knowledge, the first reported example of a molecular Cr^{III}-Er^{III} complex displaying Dexter-type energy transfer

Table 1. Photophysical parameters of the assemblies $[(\mathbf{dqp}Cr\mathbf{L1})_3Ln]^{6+}$ (Ln = Y, Er).

	Excited level	$\tilde{\nu}$ / cm^{-1}	ε_{max} / $M^{-1}cm^{-1}$	$\tau_{rad}^{Cr_3Ln}$ / ms [a]	τ_{obs} (µs) [b]		ϕ (%) [e,f]	ϕ (%) [f,h]
$[(\mathbf{dqp}Cr\mathbf{L1})_3Y]^{6+}$	$Cr(^2E)$	13738	0.95	34.79	20.90[c]	31.24	0.3	16
	$Cr(^2T_1)$	13371	0.26	78.54				
$[(\mathbf{dqp}Cr\mathbf{L1})_3Er]^{6+}$	$Cr(^2E)$	13738	0.95	32.01	7.90[c]	8.2[d]	0.3	16
	$Cr(^2T_1)$	13371	0.27	45.08				
	$Er(^4I_{13/2})$	6607	2.06	8.84	5.0[c]	9.85[d]	0.063[g]	
	$Er(^4I_{11/2})$	10248	0.66	6.33	-	-		
	$Er(^4I_{9/2})$	12544	0.09	21.80	-	-		
	$Er(^4F_{9/2})$	15356	0.88	2.58	-	-		

[a] $\tau_{rad} = 1/k_{rad}$. [b] τ_{obs} from time-resolved experiments at 293K. [c] In acetonitrile solution. [d] In the solid state. [e] In aerobic conditions. [f] λ_{exc}=435nm, using $[Cr(ddpd)_2]^{3+}$ as a reference. [g] Calculated with equation (7). [h] In anaerobic conditions. Lifetime: estimated relative uncertainty ± 10%.

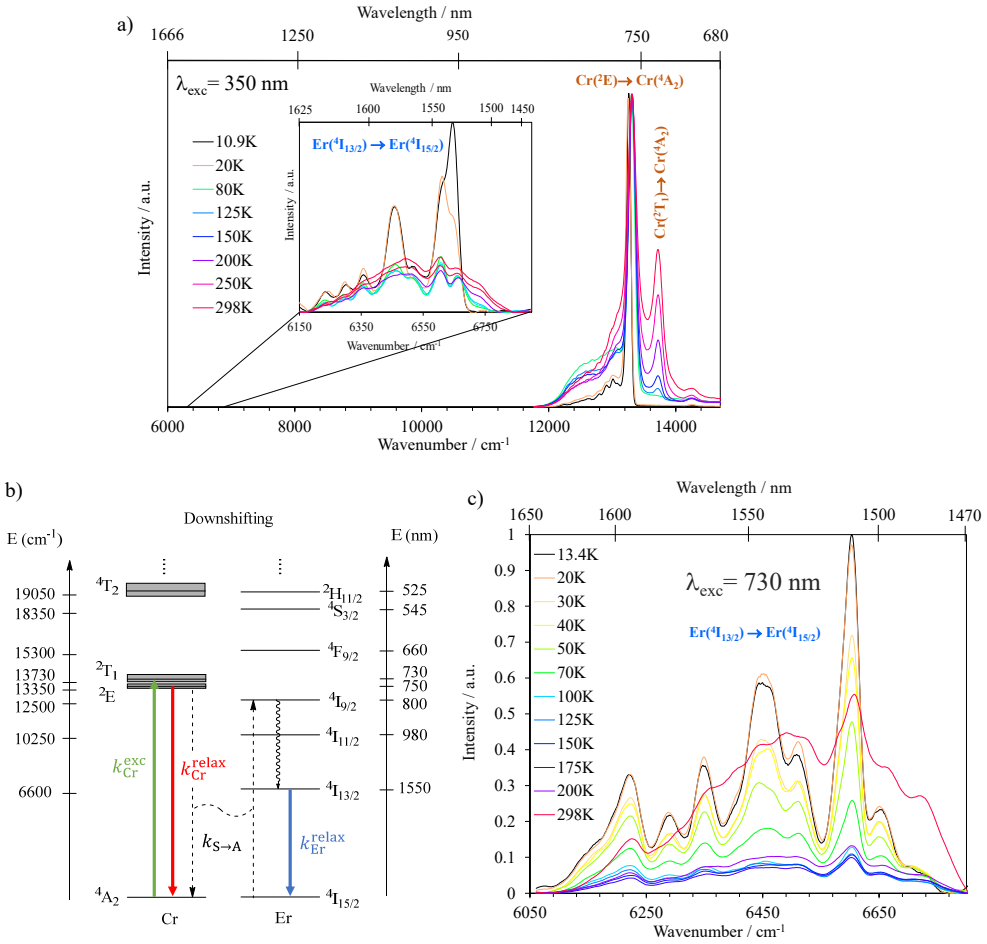

Figure 7. a) Variable temperature emission measurement of $Cr(^2T_1 \rightarrow {}^4A_2)$, $Cr(^2E \rightarrow {}^4A_2)$ and $Er(^4I_{13/2} \rightarrow {}^4I_{15/2})$ in $[(\mathbf{dqp}Cr\mathbf{L1})_3Er]^{6+}$ in the solid state with λ_{exc}=350 nm. b) Jablonski diagram for a downshifting process operating in molecular $[(\mathbf{dqp}Cr\mathbf{L1})_3Er]^{6+}$ c) Variable temperature emission measurement of in $[(\mathbf{dqp}Cr\mathbf{L1})_3Er]^{6+}$ in the solid state with λ_{exc} = 730 nm.

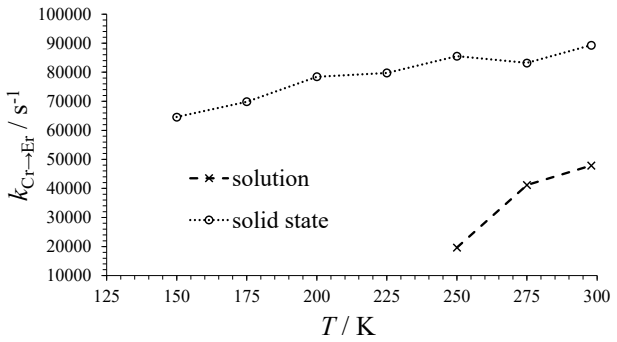

Figure 8. Variation of the EnT rate constant in the $[(\mathbf{dqp}Cr\mathbf{L1})_3Er]^{6+}$ assembly as a function of the temperature in the solid state and in solution (acetonitrile, 10^{-3} M).

Conclusion

A structurally optimized $[Cr(\mathbf{dqp})(H_2\text{-}\mathbf{L1})]^{3+}$ building block has been designed and characterized. After deprotonation of the dipicolinic acid moiety, the complex was able to bind rare earths (Y^{III} or Er^{III}) forming the hetero-tetrametallic $[(\mathbf{dqp}Cr\mathbf{L1})_3Y]^{6+}$ and $[(\mathbf{dqp}Cr\mathbf{L1})_3Er]^{6+}$ supramolecular assemblies. Valuable Er^{III}-based downshifting emission at 1550 nm upon irradiation on the spin-flip transition of the sensitizer $Cr(^2E,^2T_1\leftarrow{}^4A_2)$ at 730 nm was extensively studied at different temperatures. Time resolved experiments showed that the large EnT efficiency and rate constants are dominated by a "Dexter-type" (through-bonds) energy transfer. The intermetallic distance between the two trivalent d and f metals was increased from ~9.2 Å in triple helices CrEr and CrErCr to ~14.15 Å in the current system. Despite the longer intermetallic distance, the rate of transfer is increased from 232-456 s^{-1} to 89300 s^{-1} reaching the range reported for 4d-4f and 5d-4f systems which benefit from the expansion of the d-orbitals accompanying the removal of the primogenic effect.[63] This is the first example of a d-f heterometallic molecular system using chromium for which "Dexter-type" energy transfer over nanometric distance is observed.

Experimental section

No uncommon hazards are noted.

Solvents and starting materials. Reagent grade acetonitrile (ACN) was distilled from CaH_2. All other chemicals were purchased from commercial suppliers and used without further purification. Silica-gel plates (Merck, 60 F254) were used for thin-layer chromatography and preparative column chromatography was performed using SiliaFlash® silica gel P60 (0.04-0.063 mm).

Spectroscopic and analytical measurements. ^1H and ^{13}C NMR spectra were recorded at 298 K on a Bruker Avance 400 MHz spectrometer. Spectrophotometric titrations were performed with a J&M diode array spectrometer (Tidas series) connected to an external computer. Mathematical treatment of the spectrophotometric titrations was performed with factor analysis and with ReactLab™ Equilibria[A1-A4] (previously Specfit/32). Pneumatically assisted electrospray (ESI) mass spectrum was recorded on an Applied Biosystems API 150EX LC/MS System equipped with a Turbo Ionspray source®. High Resolution Mass Spectra were recorded on a Xevo G2-TOF HRMS instrument equipped with a Zspray™ Lockspray™ ESI/APCI/ESCi® electrospray by Waters™. Elemental analyses were performed by K. L. Paglia from the Microchemical Laboratory of the University of Geneva. Solution state absorption spectra were recorded using a Lambda 1050 Perkin Elmer spectrometer (quartz cell path length 1 cm, 1 mm or 0.2 mm, 250-1600 nm domain). Solid state absorption spectra were recorded using a Lambda 900 Perkin Elmer spectrometer (using quartz plates). Emission spectra (excitation at 355 nm) and excitation spectra were recorded, with a Fluorolog (Horiba Jobin-Yvon), equipped with iHR320, a Xenon lamp 450-Watt Illuminator (FL-1039A/40A), a water-cooled photo multiplier tube (PMT Hamamatsu R2658 or R928) for the 250-850 nm range and a liquid nitrogen cooled photo multiplier tube (Hamamatsu IR PMT H10330-75) for the 800-1650 nm range. Both detectors are corrected for the spectral response of the system. Emission spectra (excitation at 730 nm) was recorded with a MDL-III-730-1.5W as light source connected to a PSU-III-LED power supply. Variable temperature measurements were done using a closed-cycle cryosystem (Janis, CCS-900/204N) with the sample sitting in the exchange gas (helium) to achieve efficient cooling. The samples were put in 2 mm diameter cylindrical quartz cuvettes or between two flat quartz plates. The cuvettes were sealed with fast drying silver agar gel and parafilm to then be mounted on a metallic copper sample holder. For time-resolved experiments, the decay curves were recorded from previously excited samples, with a photomultiplier (Hamamatsu R2658 or R928 or Hamamatsu IR PMT H10330-75) and a digital oscilloscope (Tektronix MDO4104C). Pulsed excitation at 355 nm was obtained with the third harmonic of a pulsed Nd:YAG laser (Quantel Qsmart 850).

ASSOCIATED CONTENT

The Supporting Information is available free of charge at https://pubs.acs.org/doi/XXX.

Complete experimental details, complexes syntheses and characterizations, photophysical data (PDF). CCDC 2361450 and 2361449 contains the supplementary crystallographic data for ligand **10** and complex $[Cr(\mathbf{dqp})(H_2\text{-}\mathbf{L1})](CF_3SO_3)_3\cdot 3.5H_2O$ respectively. These data can be obtained free of charge from The Cambridge Crystallographic Data Centre via www.ccdc.cam.ac.uk/structures

AUTHOR INFORMATION

Corresponding Author

Juan-Ramón Jiménez - *Departamento de Química inorgánica, Facultad de Ciencias, Universidad de Granada and Unidad de Excelencia en Química (UEQ), Avda. Fuente Nueva s/n, 18071, Granada, Spain.*
Email: jrjimenez@ugr.es

Claude Piguet - *Department of Inorganic and Analytical Chemistry. University of Geneva, 30 quai E. Ansermet CH-1211 Geneva 4 (Switzerland)*; *orcid.org/0000-0001-7064-8548*
Email: Claude.Piguet@unige.ch

Authors

Maxime Poncet - *Department of Inorganic and Analytical Chemistry. University of Geneva, 30 quai E. Ansermet CH-1211 Geneva 4 (Switzerland)*.

Céline Besnard - *Laboratory of Crystallography, University of Geneva, 24 quai E. Ansermet, CH-1211 Geneva 4, Switzerland.*

Author Contributions

All authors have given approval to the final version of the manuscript.

Funding Sources

This work is supported through grants from the Swiss National Science Foundation (grant 200020_207313).

Notes

The authors declare no conflict of interest.

ACKNOWLEDGMENT

This work is supported through grants from the Swiss National Science Foundation (grant 200020_207313). J.R.J. thanks Ministerio de Ciencia Innovación y Universidades for a Ramón y Cajal contract (grant RYC2022-037255-I) funded by MCIN/AEI/10.13039/501100011033 and FSE+.

REFERENCES

(1) Wu, W.; Zhang, X.; Kornienko, A. Y.; Kumar, G. A.; Yu, D. C.; Emge, T. J.; Riman, R. E.; Brennan, J. G., Efficient NIR Emission from Nd, Er, and Tm Complexes with Fluorinated Selenolate Ligands. *Inorg. Chem.* **2018**, *57*, 1912-1918.

(2) Sun, G. T.; Xie, Y.; Sun, L. N.; Zhang, H. J., Lanthanide upconversion and downshifting luminescence for biomolecules detection. *Nanoscale Horiz.* **2021**, *6*, 766-780.

(3) Yang, Y. J.; Tu, D. T.; Zhang, Y. Q.; Zhang, P.; Chen, X. Y., Recent advances in design of lanthanide-containing NIR-II luminescent nanoprobes. *Iscience* **2021**, *24*. 102062.

(4) Bünzli, J.-C. G., Lanthanide light for biology and medical diagnosis. *J. Luminesc.* **2016**, *170*, 866-878.

(5) Ye, H. Q.; Li, Z.; Peng, Y.; Wang, C. C.; Li, T. Y.; Zheng, Y. X.; Sapelkin, A.; Adamopoulos, G.; Hernández, I.; Wyatt, P. B.; Gillin, W. P., Organo-erbium systems for optical amplification at telecommunications wavelengths. *Nat. Mater.* **2014**, *13*, 382-386.

(6) Bünzli, J.-C. G., Applications of Rare Earths in *The lanthanides and Actinides, Synthesis, Reactivity, Properties and Applications*, Liddle, S. T.; Mills, D. P.; Natrajan, L. S., Eds, World Scientific, London, 2022, chap. 17, pp 633-686.

(7) Bünzli, J.-C. G., On the design of highly luminescent lanthanide complexes. Elsevier: 2015; Vol. 293, pp 19-47.

(8) Comby, S.; Bünzli, J.-C. G., Lanthanide near-Infrared Luminescence in Molecular Probes and Devices. In *Handbook on the Physics and Chemistry of Rare Earths*, GschneidnerJr, K. A.; Bünzli, J.-C. G.; Pecharsky, V. K., Eds. Elsevier Science: Amsterdam, 2007; Vol. 37, pp 217-470.

(9) Ward, M. D., Mechanisms of sensitization of lanthanide(III)-based luminescence in transition metal/lanthanide and anthracene/lanthanide dyads. *Coord. Chem. Rev.* **2010**, *254*, 2634-2642.

(10) Northrop, B. H.; Zheng, Y.-R.; Chi, K.-W.; Stang, P. J., Self- Organization in Coordination-Driven Self-Assembly. *Acc. Chem. Res.* **2009**, 42, 1554−1563.

(11) Chakrabarty, R.; Mukherjee, P. S.; Stang, P. J., Supramolecular Coordination: Self-Assembly of Finite Two- and Three-dimensional Ensembles. *Chem. Rev.* **2011**, *111*, 6810−6918.

(12) Thomas, J. A. Metal Ion Directed Self-Assembly of Sensors for Ions, Molecules and Biomolecules. *Dalton Trans.* **2011**, *40*, 12005−12016.

(13) Mede, T.; Jäger, M.; Schubert, U. S., 'Chemistry-on-the-complex': Functional Ru(II) polypyridyl-type sensitizers as divergent building blocks. *Chem. Soc. Rev.* **2018**, *47*, 7577−7627.

(14) Datta, S.; Saha, M. L.; Stang, P. J., Hierarchical Assemblies of Supramolecular Coordination Complexes. *Acc. Chem. Res.* **2018**, *51*, 2047−2063.

(15) Agosti, A.; Kuna, E.; Bergamini, G., Divergent terpyridine-Based Coordination for the Construction of Photoactive Supramolecular Structures. *Eur. J. Inorg. Chem.* **2019**, 577−584.

(16) Li, F.; Lindoy, L. F., Metalloligand Strategies for Assembling Heteronuclear Nanocages - Recent Developments. *Aust. J. Chem.* **2019**, *72*, 731−741.

(17) Wang, S. C.; Cheng, K. Y.; Fu, J. H.; Cheng, Y. C.; Chan, Y. T., Conformational Regulation of Multivalent Terpyridine Ligands for Self-Assembly of Heteroleptic Metallo-Supramolecules. *J. Am. Chem. Soc.* **2020**, *142*, 16661−16667.

(18) Balzani, V.; Ceroni, P.; Credi, A.; Venturi, M. Ruthenium Tris(bipyridine) Complexes: Interchange Between Photons and Electrons in Molecular-scale Devices and Machines. *Coord. Chem. Rev.* **2021**, *433*, 213758.

(19) Büldt, L. A.; Wenger, O. S., Chromium complexes for luminescence, solar cells, photoredox catalysis, upconversion, and phototriggered NO release. *Chem. Sci.* **2017**, *8*, 7359-7367.

(20) Forster, C.; Heinze, K., Photophysics and photochemistry with Earth-abundant metals - fundamentals and concepts. *Chem. Soc. Rev.* **2020**, *49*, 1057-1070.

(21) Wegeberg, C.; Wenger, O. S., Luminescent First-Row Transition Metal Complexes. *JACS Au* **2021**, *1*, 1860-1876.

(22) Jimenez, J.-R.; Doistau, B.; Poncet, M.; Piguet, C., Heteroleptic Trivalent Chromium in Coordination Chemistry: Novel Building Blocks for Addressing Old Challenges in Multimetallic Luminescent Complexes. *Coord. Chem. Rev.* **2021**, *434*, 213750.

(23) Brayshaw, P. A.; Bünzli, J.-C. G.; Froidevaux, P.; Harrowfield, J. M.; Kim, Y.; Sobolev, A. N., Synthetic, structural and spectroscopic studies on solids containing tris(dipicolinato) rare earth anions and transition or main group metal cations. *Inorg. Chem.* **1995**, *34*, 2068-2076

(24) Sanada, T.; Suzuki, T.; Yoshida, T.; Kaizaki, S., heterodinuclear complexes containing d- and f-block elements: synthesis, structural characterization and metal-metal interactions of novel chromium(III)-lanthanide(III) compounds bridged by oxalate. *Inorg. Chem.* **1998**, *37*, 4712-4717.

(25) Subhan, M. A.; Suzuki, T.; Kaizaki, S., Stereospecific assembly of chiral Λ-Cr(III)-Δ-Ln(III) oxalato bridged dinuclear 3d-4f complexes (Ln = Yb, Dy) and near infrared dichroism in the 4f-4f transitions. *J. Chem. Soc., Dalton Trans.* **2001**, 492-497.

(26) Subhan, M. A.; Suzuki, T.; Kaizaki, S., Solution NIR CD and MCD in 4f-4f transitions of a series of chiral 3d-4f dinuclear complexes: X-ray structures of (D-L)-[(acac)2Cr(III)(m-ox)Ln(IIII)(HBpz3)2] (Ln = Sm, Ho, Er). *J. Chem. Soc., Dalton Trans.* **2002**, 1416-1422.

(27) Cantuel, M.; Bernardinelli, G.; Imbert, D.; Bünzli, J.-C. G.; Hopfgartner, G.; Piguet, C., A kinetically inert and optically active Cr(III) partner in thermodynamically self-assembled heterodimetallic non-covalent d-f podates. *J. Chem. Soc., Dalton Trans.* **2002**, 1929-1940.

(28) Subhan, M. A.; Nakata, H.; Suzuki, T.; Choi, J.-H.; Kaizaki, S., Simultaneous observation of low temperature 4f-4f and 3d-3d emission spectra in a series of Cr(III)oxLn(III) assembly. *J. of. Luminesc.* **2003**, *101*, 307-315.

(29) Imbert, D.; Cantuel, M.; Bünzli, J.-C. G.; Bernardinelli, G.; Piguet, C., Extending lifetimes of lanthanide-based near-infrared emitters (Nd, Yb) in the millisecond range through Cr(III) sensitization in discrete bimetallic edifices. *J. Am. Chem. Soc.* **2003**, *125*, 15698-15699.

(30) Cantuel, M.; Bernardinelli, G.; Muller, G.; Riehl, J. P.; Piguet, C., The first enantiomerically pure helical noncovalent tripod for assembling nine-coordinate lanthanide(III) podates. *Inorg. Chem.* **2004**, *43*, 1840-1849.

(31) Torelli, S.; Imbert, D.; Cantuel, M.; Bernardinelli, G.; Delahaye, S.; Hauser, A.; Bünzli, J.-C. G.; Piguet, C., Tuning the Decay Time of Lanthanide-Based Near Infrared Luminescence from Micro- to Milliseconds through d-f Energy Transfer in Discrete Heterobimetallic Complexes. *Chem. Eur. J.* **2005**, *11*, 3228-3242.

(32) Cantuel, M.; Gumy, F.; Bünzli, J.-C. G.; Piguet, C., Encapsulation of labile trivalent lanthanides into a homobimetallic chromium(III)-containing triple-stranded helicate. Synthesis, Characterization, and divergent intramolecular energy transfers. *Dalton Trans.* **2006**, 2647-2660.

(33) Lazarides, T.; Davies, G. M.; Adams, H.; Sabatini, C.; Barigelletti, F.; Barbieri, A.; Pope, S. J. A.; Faulkner, S.; Ward, M. D., Ligand-field excited states of hexacyanochromate and hexacyanocobaltate as sensitisers for near-infrared luminescence from Nd(III) and Yb(III) in cyanide-bridged d–f assemblies. *Photochem. Photobiol. Sci.* **2007**, *6*, 1152-1157.

(34) Xu, H.-B.; Li, J.; Zhang, L. Y.; Huang, X.; Li, B.; Chen, Z.-N., Structures and photophysical properties of homo- and heteronuclear lanthanide(III) complexes with bridging 2-methyl-8-hydroxylquinoline (HMq) in the M-phenol mode. *Crystal Growth & Design* **2010**, *10*, 4101-4108.

(35) McRobbie, A.; Sarwar, A. R.; Yeninas, S.; Nowell, H.; Baker, M. L.; Allan, D.; Luban, M.; Muryn, C. A.; Pritchard, R. G.; Prozorov, R.; Timco, G. A.; Tuna, F.; Whitehead, G. F. S.; Winpenny, R. E. P., Chromium chains as polydentate fluoride ligands for lanthanides. *Chem. Commun.* **2011**, *47*, 6251-6253.

(36) Kalmbach, J.; Wang, C.; You, Y.; Forster, C.; Schubert, H.; Heinze, K.; Resch-Genger, U.; Seitz, M., Near-IR to Near-IR Upconversion Luminescence in Molecular Chromium Ytterbium Salts. *Angew. Chem. Int. Ed.* **2020**, 59, 18804-18808.

(37) Doistau, B.; Jimenez, J. R.; Guerra, S.; Besnard, C.; Piguet, C., Key Strategy for the Rational Incorporation of Long-Lived NIR Emissive Cr(III) Chromophores into Polymetallic Architectures. *Inorg. Chem.* **2020**, *59*, 1424-1435.

(38) Doistau, B.; Jimenez, J. R.; Daku, L. M. L.; Piguet, C., Complex-as-Ligand Strategy as a Tool for the Design of a Binuclear Nonsymmetrical Chromium(III) Assembly: Near-Infrared Double Emission and Intramolecular Energy Transfer. *Inorg. Chem.* **2022**, *61*, 11023-11031.

(39) Waki, M.; Abe, H.; Inouye, M., Helix Formation in Synthetic Polymers by Hydrogen Bonding with Native Saccharides in Protic Media. *Chem. Eur. J.* **2006**, *12*, 7839-7847.

(40) Jäger, M.; Kumar, R. J.; Görls, H.; Bergquist, J.; Johansson, O., Facile Synthesis of Bistridentate Ru^{II} Complexes Based on 2,6-Di(quinolin-8-yl)pyridyl Ligands: Sensitizers with Microsecond 3MLCT Excited State Lifetimes. *Inorg. Chem.* **2009**, *48*, 3228-3238.

(41) Norris, M. R.; Concepcion, J. J.; Glasson, C. R. K.; Fang, Z.; Lapides, A. M.; Ashford, D. L.; Templeton, J. L.; Meyer, T. J., Synthesis of Phosphonic Acid Derivatized Bipyridine Ligands and Their Ruthenium Complexes. *Inorg. Chem.* **2013**, *52*, 12492-12501.

(42) Ashford, D. L.; Brennaman, M. K.; Brown, R. J.; Keinan, S.; Concepcion, J. J.; Papanikolas, J. M.; Templeton, J. L.; Meyer, T. J., Varying the Electronic Structure of Surface-Bound Ruthenium(II) Polypyridyl Complexes. *Inorg. Chem.* **2015**, *54*, 460-469.

(43) Doistau, B.; Collet, G.; Acuna Bolomey, E.; Sadat-Noorbakhsh, V.; Besnard, C.; Piguet, C., Heteroleptic Ter-Bidentate Cr(III) Complexes as Tunable Optical Sensitizers. *Inorg. Chem.* **2018**, *57*, 14362-14373.

(44) Richardson, C.; Reed, C. A., Synthesis of meso-Extended Tetraarylporphyrins. *J. Org. Chem.* **2007**, *72*, 4750-4755.

(45) Nettekoven, M.; Jenny, C., The Development of a Practical and Reliable Large-Scale Synthesis of 2,6-Diamino-4-bromopyridine, *Organic Process Research & Development* **2003**, *7*, 38-43.

(46) Jimenez, J.-J.; Doistau, B.; Besnard, C.; Piguet, C., Versatile Heteroleptic Bis-Terdentate Cr(III) Chromophores Displaying Room Temperature Millisecond Excited State Lifetimes. *Chem. Commun.* **2018**, *54*, 13228-13231.

(47) Jiménez, J.-R.; Poncet, M.; Doistau, B.; Besnard, C.; Piguet, C., Luminescent polypyridyl heteroleptic Cr^{III} complexes with high quantum yields and long excited state lifetimes. *Dalton Trans.* **2020**, *49*, 13528-13532.

(48) Barker, K. D.; Barnett, K. A.; Connel, S. M.; Glaeser, J. W.; Wallace, A. J.; Wildsmith, J.; Herbert, B. J.; Wheeler, J. F.; Kane-Maguire, N. A. P., Synthesis and characterization of heteroleptic $[Cr(diimine)_3]^{3+}$ complexes, *Inorg. Chim. Acta* **2001**, *316*, 41-49.

(49) Jimenez, J. R.; Doistau, B.; Cruz, C. M.; Besnard, C.; Cuerva, J. M.; Campana, A. G.; Piguet, C., Chiral Molecular Ruby $[Cr(dqp)_2]^{3+}$ with Long-Lived Circularly Polarized Luminescence", *J Am Chem Soc* **201**9, *141*, 13244-13252.

(50) Jiménez, J.-R.; Poncet, M.; Míguez-Lago, S.; Grass, S.; Lacour, J.; Besnard, C.; Cuerva, J. M.; Campaña, A. G.; Piguet, C., Bright Long-Lived Circularly Polarized Luminescence in Chiral Chromium(III) Complexes, *Angew. Chem. Int. Ed.* **2021**, *60*, 10095-10102.

(51) Sinha, N.; Yaltseva, P.; Wenger, O. S., The Nephelauxetic Effect Becomes an Important Design Factor for Photoactive First-Row Transition Metal Complexes. *Angew. Chem. Int. Ed.* **2023**, *62*, e202303864.

(52) Wenger, O. S., Photoactive Complexes with Earth-Abundant Metals. *J. Am. Chem. Soc.* **2018**, *140*, 13522-13533.

(53) Benchohra, A.; Chong, J. L.; Cruz, C. M.; Besnard, C.; Guénée, L.; Rosspeintner, A.; Piguet, C., Additional Insights into the Design of Cr(III) Phosphorescent Emitters Using 6-Membered Chelate Ring Bis(imidazolyl) Didentate Ligands. *Inorg. Chem.* **2024**, *63*, 3617−3629.

(54) Maeder, M.; King, P., Analysis of chemical processes, determination of the reaction mechanism and fitting of equilibrium and rate constants. In *Chemometrics in Practical Applications*, Varmuza, K., Ed. INTECH: 2012; pp 41-62.

(55) Gampp, H.; Maeder, M.; Meyer, C. J.; Zuberbuehler, A. D., Calculation of equilibrium constants from multiwavelength spectroscopic data. III. Model-free analysis of spectrophotometric and ESR titrations. *Talanta* **1985**, *32*, 1133-1139.

(56) Gampp, H.; Maeder, M.; Meyer, C. J.; Zuberbuehler, A. D., Calculation of equilibrium constants from multiwavelength spectroscopic data - IV. Model-free least-squares refinement by use of evolving factor analysis. *Talanta* **1986**, *33*, 943-951.

(57) Clifford, S.; Lawrance, G. A.; Neuhold, Y.-M.; Maeder, M., Conjoint analysis of kinetic and equilibrium data for mechanistic elucidation in polynuclear complexation

reactions, exemplified by metal(II) helicate complex formation. *Aust. J. Chem.* **2010**, *63*, 141-144.

(58) Grenthe, I., Stability Relationships among Rare Earth Dipicolinates. *J. Am. Chem. Soc.* **1961**, *83*, 360-364.

(59) Piguet, C., Microscopic Thermodynamic Descriptors for Rationalizing Lanthanide Complexation Processes. In *Handbook on the Physics and Chemistry of Rare Earths*, GschneidnerJr, K. A.; Bünzli, J.-C. G.; Pecharsky, V. K., Eds. Elsevier Science: Amsterdam, 2015; Vol. 47, pp 209-271.

(60) Alderighi, L.; Gans, P.; Ienco, A.; Peters, D.; Sabatini, A.; Vacca, A., Hyperquad simulation and speciation (HySS): a utility program for the investigation of equilibria involving soluble and partially soluble species. *Coord. Chem. Rev.* **1999**, *184*, 311-318.

(61) Strickler, S. J.; Berg, R. A., Relationship between Absorption Intensity and Fluorescence Lifetime of Molecules. *J. Chem. Phys.* **1962**, *37*, 814-822.

(62) Angulo, G.; Grampp, G.; Rosspeintner, A., Recalling the appropriate representation of electronic spectra. *Spectrochim. Acta Part a-Molecular and Biomolecular Spectroscopy* **2006**, *65*, 727-731.

(63) McCusker, J. K., Electronic structure in the transition metal block and its implications for light harvesting. *Science* **2019**, *363*, 484-488.

(64) Hulliger, F.; Landolt, M.; Vetsch, H., Rare-earth ferricyanides and chromicyanides $LnT(CN)_6 \cdot nH_2O$, *Journal of Solid State Chemistry* **1976**, *18* (3), 283-291.

(65) Estrader, M.; Ribas, J.; Tangoulis, V.; Solans, X.; Font-Bardía, M.; Maestro, M.; Diaz, C., Synthesis, Crystal Structure, and Magnetic Studies of One-Dimensional Cyano-Bridged Ln3+─Cr3+ Complexes with bpy as a Blocking Ligand, *Inorg. Chem.* **2006**, *45* (20), 8239-8250.

(66) Andruh, M.; Costes, J.-P.; Diaz, C.; Gao, S., 3d-4f combined chemistry: synthetic strategies and magnetic properties, *Inorg. Chem.* **2009**, *48*, 3342-3359.

(67) Birk, T.; Pedersen, K. S.; Thuesen, C. A.; Weyhermueller, T.; Scha-Magnusen, M.; Piligkos, S.; Weihe, H.; Mossin, S.; Evangelisti, M.; Bendix, J., Fluoride bridges as structure-directing motifs in 3d-4f cluster chemistry, *Inorg. Chem.* **2012**, *51*, 5435-5443.

(68) Zare, D.; Suffren, Y.; Guénée, L.; Eliseeva, S. V.; Nozary, H.; Aboshyan-Sorgho, L.; Petoud, S.; Hauser, A.; Piguet, C., Smaller than a nanoparticle with the design of discrete polynuclear molecular complexes displaying near-infrared to visible upconversion, *Dalton Trans.* **2015**, *44*, 2529-2540.

(69) Golesorkhi, B.; Naseri, S.; Guenee, L.; Taarit, I.; Alves, F.; Nozary, H.; Piguet, C., Ligand-Sensitized Near-Infrared to Visible Linear Light Upconversion in a Discrete Molecular Erbium Complex, *J. Am. Chem. Soc.* **2021**, *143* (37), 15326-15334.

(70) Aboshyan-Sorgho, L.; Cantuel, M.; Petoud, S.; Hauser, A.; Piguet, C., Optical sensitization and upconversion in discrete polynuclear chromium-lanthanide complexes, *Coord. Chem. Rev.* **2012**, *256*, 1644-1663.

(71) Bolvin, H.; Fürstenberg, A.; Golesorkhi, B.; Nozary, H.; Taarit, I.; Piguet, C., Metal-Based Linear Light Upconversion Implemented in Molecular Complexes: Challenges and Perspectives, *Acc. of Chem. Res.* **2022**, *55* (3), 442-456.

SYNOPSIS TOC

The remarkable kinetic inertness of trivalent chromium cations allows the stepwise preparation of the heteroleptic [Cr**dqp**(H_2-**L1**)]$^{3+}$ building block which can work as 'complex-as-ligand' for the self-assembly of dimetallic [(**dqp**Cr**L1**)$_3$Er]$^{6+}$ under basic conditions. The latter supramolecular architecture collects red light (730 nm) for its downshifting toward the infrared domain (1550 nm).